Physical Human-Aerial Robot Interaction and Collaboration: Exploratory Results and Lessons Learned

Amr Afifi[1], Gianluca Corsini[3], Quentin Sable[1], Youssef Aboudorra[1], Daniel Sidobre[3], Antonio Franchi[1,2,3]

***Abstract*— In this work, we present, a first of its kind, physical human-aerial robot interaction (pHARI) experiment, with an articulated aerial manipulator (AM). The robotic platform is a fully-actuated multi-rotor aerial vehicle (MRAV) with fixedly-tilted propellers endowed with a 3degree of freedom (DoF) robotic arm. We implemented a state-of-the-art control architecture composed of a feedback linearization motion controller, an admittance filter and a hybrid wrench observer. The experiments prove the viability of a new use case in aerial robotics, namely pHARI. The experimental results also shed light on the limitations of the current state-of-the-art and provide insights into possible research directions. The video of the experiments, which is available at https://youtu.be/LrQxXbQ5IHc, shows an experiment simulating work at height, where a human manually guides an AM and then attaches a tool to its end effector (EE).**

Fig. 1. Snapshot from the physical interaction experiment between the human and the AM. The human hooks a tool to the robot end effector and proceeds to reposition the aerial platform according to their preference by guiding the end effector through physical contact.

I. Introduction

Aerial robots (ARs) that can interact physically with the environment are increasingly considered in aerial robotics literature with emergent industrial use cases. From an application perspective, these robots have the potential to automate work at height. One prominent example of an application is non-destructive testing (NDT) [1] at height. Another interesting use of ARs is performing maintenance and inspection tasks of large infrastructures, such as power lines and construction sites [2]. Due to the complexity in operating in these types of environments, the dexterity and perception capabilities of the human workers are invaluable. Therefore, in order for ARs to provide useful functionality in these scenarios, they must be able to coexist and collaborate with their human partners. In other words, the ARs should become *aerial co-workers (ACWs)*, thus useful components in these human populated workspace.

Work at height is both physically and cognitively demanding. Human operators in these settings have constrained mobility and their work activities can lead to un-ergonomic postures. Physically-interactive ARs provide an opportunity to improve the working conditions in these scenarios. We envision that these vehicles can safely and effectively interact with human workers, e.g., by delivering tools, or by collaboratively transporting objects. These tasks will require an exchange of forces between the AR and the human, which should guarantee safety and allow for an intuitive interaction.

In this work, we take a step towards realizing a physically-interactive aerial co-working robot. We perform experiments involving physical interaction in the context of a tool-delivery scenario at height. In the conducted experiments, the human exchanges forces directly with an articulated AM, without intermediate elements such as cables or passive joints. Additionally, a small payload is exchanged. These experiments go beyond the state of the art in physical human-aerial robot interaction (pHARI) and consequently provide insights into further research directions aimed at realizing ACWs.

The literature in aerial physical interaction presents a wide array of platform designs that can improve the robot capabilities to perform physical interaction, which is essential for the aerial co-worker. In [3], an under-actuated quadrotor is combined with a manipulator consisting of both active and passive elements which allow the robot to handle impacts. Alternatively, in [4], a fully-actuated hexarotor design is proposed featuring fixedly-tilted propellers. This allows the hexarotor to independently exert forces and torques in all directions. The platform used in this work belongs to the class of fully-actuated multi rotors with fixedly-tilted propellers, additionally equipped with a robotic arm. For a detailed review on AR designs, we refer the reader to [5].

[1]Robotics and Mechatronics lab, Faculty of Electrical Engineering, Mathematics & Computer Science, University of Twente, Enschede, The Netherlands a.n.m.g.afifi@utwente.nl, y.a.l.a.aboudorra@utwente.nl, q.l.g.sable@utwente.nl, a.franchi@utwente.nl

[2]Department of Computer, Control and Management Engineering, Sapienza University of Rome, 00185 Rome, Italy antonio.franchi@uniroma1.it

[3]LAAS-CNRS, UPS, Université de Toulouse, Toulouse, France gianluca.corsini@laas.fr, daniel.sidobre@laas.fr, antonio.franchi@laas.fr

This work was partially funded by the ANR, under the Projects ANR-18-CE33-0001 'The flying coworker', and by the European Commission project H2020 AERIAL-CORE (EC 871479).

Moreover, there is a rich literature of control methods in aerial physical interaction comprising variants of impedance and/or hybrid force motion control. These methods have been verified experimentally on different types of multi-rotor aerial vehicles (MRAVs). To give a few examples, in [6], an impedance controller is developed for a quadrotor manipulator system. In [7] instead, a fully-actuated hexarotor performs tasks requiring physical interaction such as peg-in-hole and push-and-slide. In [8], a Nonlinear Model Predictive Controller is used to perform hybrid force motion tasks. In [9], a Port-Hamiltonian approach is used to develop passive controller for physically-interactive ARs. For a comprehensive review on the advances in aerial manipulation, the interested reader can refer to [10].

Despite an extensive literature exists on aerial physical interaction, the same can not be said on the topic of aerial co-workers and pHARI. The idea has only been considered a few times in the literature. In [11], the suitability of admittance control in pHARI is demonstrated using a quadrotor. In that work, the platform does not include any additional degree of freedom (DoF) such as those offered by a robotic arm. In [12], the authors address a human-guiding use case consisting of a quadrotor guiding a human to a location via cables and by resorting to admittance control.

Our main contribution is demonstrating a contextually-rich physical interaction scenario between a human and a complex AR platform. The work exploits the state-of-the-art methods in aerial physical interaction in this new use case, shedding a light on new challenges for interactive ACWs.

The paper is organized as follows. Sec. II introduces the hardware platform used in the experiments and highlights why its particular design is advantageous in pHARI. Sec. III presents the system modelling and the controller design. Sec. IV provides details on the experimental setup. Sec. V describes the conducted experiments and the results obtained. Lastly, a discussion and conclusions follow in Sec. VI.

II. Aerial Co-Worker Platform

In this section, we present our in-house developed AM. The system consists of a MRAV with a 3-DoF robotic manipulator arm attached to its base.

The MRAV has six tilted rotors rendering it a fully-actuated system, with the ability to generate 6D wrench to independently control its full pose. This is important in order to control the AR position and orientation, for example, relative to a human. Such ability is impossible with standard underactuated/collinear multirotors.

A fixedly-attached end effector (EE) would be enough for the MRAV to obtain 6D physical interaction, as done in [7]. However, the possible achievable orientations would be limited by the input saturation of the thrusters which does not ensure gravity compensation for all the possible orientations of the main body. By using instead the 3-DoF robotic manipulator we can increase the orientation workspace of the EE and gain extra redundancy which can be used for additional objectives.

Fig. 2. Design of the AM: MRAV with a 3-DoFs robotic manipulator arm attached to its base, right: side view showing the end effector (robotic gripper) tilted in the side plane, left: frontal view showing tilting along the front plane. Notice the close up on the differential mechanism at the depicted different tilt angles.

The first two DoF of robotic arm are produced by a geared differential mechanism which uses the combination of two attached servo motors. The third DoF is controlled directly by a third servo motor, see Fig. 2. Using servo motors to control the robotic arm has implications on the interaction controller which are discussed in Sec. III.

III. Modelling and Controller design

In this section, we first provide the model of the AM, and later we present the structure of its control architecture.

As mentioned in Sec. II, the robotic arm is controlled via servo motors through position or velocity commands. In robotics, it is a commonly-used assumption that servo-controlled arms can precisely track the reference commands and reject any external disturbance [13]. Consequently, we focus on modeling only the MRAV and we treat the coupling effects induced by the arm motion as external disturbances in the dynamical model of the aerial robot. To compute their intensity and take them into account in the AR dynamics, that will be introduced shortly, we rely on the Newton-Euler (NE) formalism as explained in [14].

A. MRAV modeling

The MRAV is modeled as a rigid body of mass $m_b \in \mathbb{R}^+$ and inertia $J_b \in \mathbb{R}^{3\times3}$. To achieve fully actuation, it is equipped with $n_p = 6$ motor-propeller actuators fixedly tilted with respect to (w.r.t.) the main body [7].

As shown in Fig. 3, we define a body frame $\mathcal{F}_b$ having its origin O_b attached to the center of mass (CoM) of the base, and its axes respectively denoted by x_b, y_b, z_b. Similarly, we define an inertial frame $\mathcal{F}_w$.

The position of O_b in $\mathcal{F}_w$ is denoted by $\underline{p}_b^w \in \mathbb{R}^3$, while the orientation of $\mathcal{F}_b$ w.r.t. $\mathcal{F}_w$ is represented by the rotation matrix $R_b^w \in SO(3)$. We then indicate with $\underline{v}_b^w \in \mathbb{R}^3$ the linear velocity of O_b expressed in $\mathcal{F}_w$, and with $\underline{\omega}_b^b \in \mathbb{R}^3$ the angular velocity of $\mathcal{F}_b$ w.r.t. $\mathcal{F}_w$ and expressed in $\mathcal{F}_b$. Hereafter, to simplify the notation, we omit to report the reference frame for any vector expressed in $\mathcal{F}_w$, as well as for any rotation from a given frame to the inertial one.

The configuration of the MRAV is given by $q_b = (p_b, R_b) \in \mathbb{R}^3 \times SO(3)$, while $\nu_b = \begin{bmatrix} \underline{v}_b^\top & \underline{\omega}_b^{b\top} \end{bmatrix}^\top \in \mathbb{R}^6$ collects the linear and angular velocities.

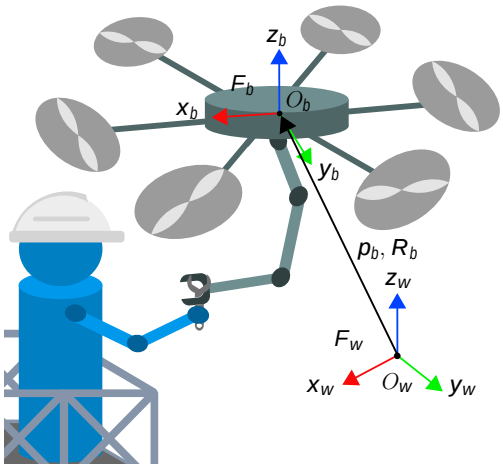

Fig. 3. Schematic depiction of the human handing over a tool to the AM co-worker, while standing on the scaffolding at height. The frames, with their origins and axes, and the position and orientation of the robot body w.r.t. $\mathcal{F}_w$ are reported.

By using the NE formalism, we can derive the equations of motion of the MRAV as follows:

$$\begin{matrix} m_b \ddot{p}_b \\ J_b \dot{\omega}_b^b \end{matrix} = \begin{matrix} m_b g z_w \\ \omega_b^b \times J_b \omega_b^b \end{matrix} + w_u + w_a + w_h; \quad (1)$$

where $\ddot{p}_b \in \mathbb{R}^3$ and $\dot{\omega}_b^b \in \mathbb{R}^3$ are respectively the linear and angular accelerations of the base, and g the gravitational constant. In (1), the quantity $w_u = [f_u^\top \; \tau_u^{b\top}]^\top \in \mathbb{R}^6$ denotes the the forces and the moments applied on the flying base by the actuators of the MRAV. The vector $w_a = [f_a^\top \; \tau_a^{b\top}]^\top \in \mathbb{R}^6$ accounts for the dynamical coupling between the MRAV and the manipulator arm. Finally, $w_h = [f_h^\top \; \tau_h^{b\top}]^\top \in \mathbb{R}^6$ takes into consideration the wrench produced by the human partner during the physical interaction transferring to the base through the manipulator.

The actual system inputs of the aerial vehicle are the individual propeller thrust forces which can be related linearly to the squares of the propeller angular rates (see [5]) denoted by $\tau_u \in \mathbb{R}^{n_p}_0$. The wrench mapping between w_u and τ_u is given by a grasp-like matrix $G_u \in \mathbb{R}^{6 \times n_p}$, i.e.,

$$w_u = G_u \tau_u; \quad (2)$$

Thanks to the full actuation assumption we have that G_u is full rank [5], which means that the wrench derivative is a vector that can have any direction[1] in $\mathbb{R}^6$, i.e., the applied wrench can be locally changed in all directions.

Eq. (1) can be written in a more compact form as follows:

$$M_b \dot{\nu}_b = h_b(\omega_b^b) + G_u \tau_u + w_a + w_h; \quad (3)$$

where $M_b = \mathrm{diag}(m_B; J_b) \in \mathbb{R}^{6 \times 6}$ is the generalised inertia tensor of the multi rotor, $\dot{\nu}_b \in \mathbb{R}^6$ collects the linear and angular accelerations of the base, $h_b(\omega_b^b) \in \mathbb{R}^6$ is the vector collecting the Centrifugal and Coriolis and gravitational effects of the MRAV.

[1]Notice that the wrench w_u cannot have any direction instead, due to the fact that $\Omega_u \in \mathbb{R}^{n_p}_{\geq 0}$.

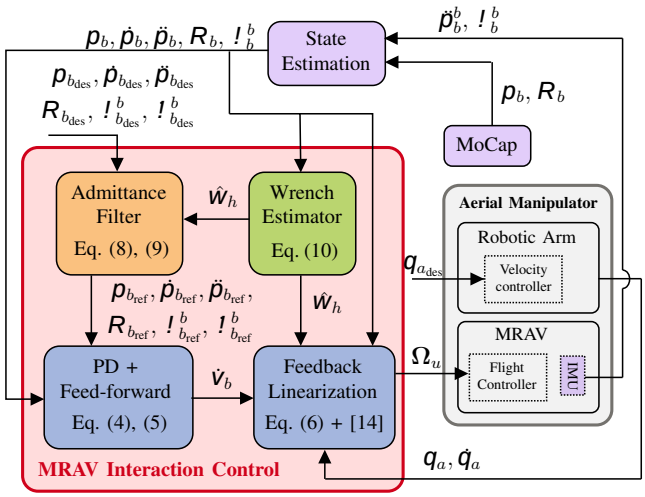

Fig. 4. Block diagram of the system architecture. In red, we highlight the modules composing the interaction controller of the MRAV. The admittance filter, modifies the desired trajectories based on the estimated external wrench, and provides the motion controller with the reference trajectories. Note, how the wrench estimator makes use of the MRAV sensor suite.

B. Manipulator Arm Modeling

As mentioned earlier, the robotic arm dynamics is accounted in the MRAV model of Eq. (3) by the quantity w_a, which we compute by resorting to the NE algorithm [14]. This quantity is function of the joint variables, precisely the joint angles, velocities and accelerations. We indicate the number of joints with n_a (thus $n_a = 3$ for our design described in Sec. II), and we then denote by $q_a \in \mathbb{R}^{n_a}$ and $\dot{q}_a \in \mathbb{R}^{n_a}$ the vectors collecting the joint angles and angular rates, respectively. Since it is usually required to move the arm at low speeds in tasks requiring physical interaction, we consider the joint accelerations $\ddot{q}_a \in \mathbb{R}^{n_a}$ to be equal to 0.

C. Control Architecture

The control architecture of the aerial manipulator comprises the physical interaction control of the MRAV and the velocity controller of the robotic arm. The former is composed of three sub-modules, namely a *Motion Controller*, a *Wrench Observer* and an *Admittance Filter*, as shown with three different colors (respectively, blue, green and orange) in the block diagram in Fig. 4.

1) Motion Controller: The first module of the control architecture is the Motion Controller, which generates the actuator commands that are fed to the system.

Firstly, we define a virtual input that is composed of a PD and feed-forward term, which has the objective to zero the tracking errors. This is achieved by the equation

$$\dot{\nu}_b^r = \begin{matrix} K_p e_p + K_v e_v + \ddot{p}_{b_{ref}} \\ K_R e_R + K_\omega e_\omega + \dot{\omega}_{b_{ref}}^b \end{matrix}; \quad (4)$$

where the error terms are computed as follows

$$\begin{matrix} e_p = p_{b_{ref}} - p_b; & & e_v = \dot{p}_{b_{ref}} - \dot{p}_b; \\ e_R = \frac{1}{2}\left(R_{b_{ref}}^\top R_b - R_b^\top R_{b_{ref}}\right)^\vee; & & e_\omega = \omega_{b_{ref}}^b - \omega_b^b. \end{matrix} \quad (5)$$

In (4), K_p, K_v, K_R, and K_ω are 3-by-3 real gain matrices, while the operator $\_^\vee$ in (5) is the inverse mapping of the skew operator [15]. The subscript "ref" in (4) and (5) is used to indicate the reference values, e.g. $p_{b_{\text{ref}}}$ is the reference of p_b.

This virtual input is then used within a feedback linearization scheme as follows

$$u = G_u^{-1}(M_b \dot{v}_b + h_b \quad w_a \quad w_h). \tag{6}$$

2) Joint Velocity Controller: The robotic arm is controlled by servo motors featuring a low-level velocity controller, and as mentioned earlier, we rely on the assumption that servo motor can track the desired joint commands precisely. In mathematical terms this translates to the following equation

$$q_a \quad q_{a_{\text{des}}}. \tag{7}$$

3) Admittance Filter: In our control scheme, the admittance filter, which is responsible for the robot interaction behavior, acts only on the MRAV trajectory. This is contrary to the usual choice of designing the interaction control at the EE level. However, since the manipulator arm is velocity-controlled, we cannot implement impedance or admittance control at the end effector, since these schemes require the ability to control the forces or the accelerations, respectively.

Therefore, we assume that the MRAV and the joint trajectories are available a priori and correspond to a desired EE pose. We can then, directly command the arm by issuing the desired joint angular rates, and assume that throughout the physical interaction phase the robotic arm is able to track precisely its set-point, cancelling out the contact wrench.

Consequently, given the desired motion, the admittance filter computes a new reference trajectory for the MRAV based on the desired interaction dynamics and the knowledge of the external wrench applied by the human on the robot. Thus, similarly to our previous work [16], the admittance filter is given by

$$M_{\text{app}} \begin{matrix} a \\ \dot{} \end{matrix} + D_{\text{app}} \begin{matrix} v \\ \end{matrix} + K_{\text{app}} \begin{matrix} p \\ R \end{matrix} = \begin{matrix} f_h \\ b \\ h \end{matrix}; \tag{8}$$

where the 6-by-6 real matrices M_{app}, D_{app}, and K_{app} are the designed apparent inertia, damping and stiffness of the system, respectively. The terms are the error vectors between the reference and the desired trajectory of the flying vehicle. They can be computed as follows

$$a = p_{b_{\text{ref}}} \quad p_{b_{\text{des}}}; \qquad \dot{} = \dot{}_{b_{\text{ref}}} \quad \dot{}_{b_{\text{des}}}; \tag{9}$$

where we omit the position, attitude, and velocity errors for the sake of conciseness. Indeed, they can be calculated in the same way as in (5) by substituting the actual state of the MRAV with the desired motion signal tasked to the robot.

4) External Wrench Estimation: To perform interaction control, we need to measure or estimate the human wrench applied on the MRAV. Therefore, the third part composing the control architecture is an External Wrench Observer, which allows estimating the forces and moments applied by the human on the robot. In this case we opted for keeping the platform more basic and using an indirect method rather than directly measuring the external wrench through the use of an external sensor, e.g., a force-torque sensor, which will be easily integrated in the framework in future works. For the wrench observer, we extended the formulation presented in [17] to account also for the wrench generated by the robotic arm. The estimated human wrench $\hat{w}_h \in \mathbb{R}^6$ is calculated as follows

$$\hat{w}_h = \begin{bmatrix} \hat{f}_h & \hat{\tau}_h^b \end{bmatrix}^\top = \tag{10}$$
$$\begin{bmatrix} \int_0^t K_{I,f} \left(m_b \ddot{p}_b + m_b g z_w \quad f_u \quad f_a \quad \hat{f}_h \right) \mathrm{d}t \\ K_{I,\tau} \left(J_b \dot{\omega}_b^b + \int_0^t \omega_b^b \times J_b \omega_b^b \quad \tau_u^b \quad \tau_a^b \quad \hat{\tau}_h^b \right) \mathrm{d}t \end{bmatrix};$$

$\hat{f}_h \in \mathbb{R}^3$ and $\hat{\tau}_h^b \in \mathbb{R}^3$ are the estimated human forces and torques, $K_{I,f}$ and $K_{I,\tau}$ are 3-by-3 real gain matrices.

IV. Experimental Setup

Here, we provide details about the experimental setup.

The robotic arm is actuated by Dynamixel motors that allow retrieving the measures of the joint angles and their velocity. The end effector of the robotic arm consists in a hook-like device that allows the human operator at height to secure the tools to be handed over. For conducting the experiments in a safe manner, the human worker wears protective gear, such as an helmet with visor, gloves, and clothing that prevents leaving any body part from being exposed. Moreover, the robot is secured by means of a cable to the ceiling of the experimental room. In this way, in case of any hardware failure, the experiment can be instantly terminated and the robot turned off without involving any danger for the human partner or damages to the platform. Furthermore, an operator placed at a ground station supervises the activities, operates the state machine of the software architecture through a joystick, and decides whether proceeding with the different states or terminating the experiments in case of any unexpected event.

A motion capture (MoCap), installed in the ceiling of the experimental room, is used to obtain the position and the attitude of the robot. Onboard sensor measurements are also available and they comprise linear accelerations and angular velocities from the IMU. All the available data are fused together in an Unscented Kalman Filter to retrieve the pose of the MRAV. In Fig. 4, the modules of the system related to the robot state estimation are highlighted in purple.

V. Experimental Results

In this section, we describe the pHARI experiment and present the results. We encourage the reader to watch the video of the experiments at https://youtu.be/LrQxXbQ5IHc.

The experiment is divided into three phases, namely the *approach*, the *interaction* and the *retreat*. These phases also constitute the three states of the state machine, each one enabling or disabling some functionality.

Initially, the AM, which is in the approach state, approaches the worker and stops in front of the human. The actual and reference position of the AR during the approach phase can be seen in the top plot in Fig. 5. In this phase, the robot motion controller is able to achieve good tracking performance of the reference set-point see Fig. 6.

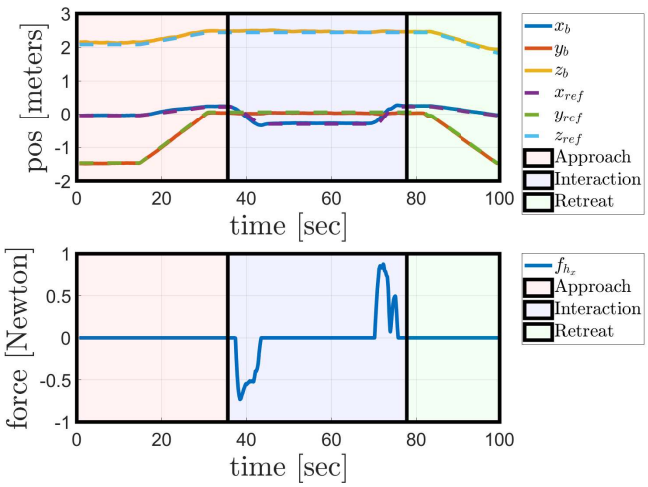

Fig. 5. The top and bottom plots are divided into three different highlighted regions representing the three phases of the experiment. In the top plot, we report the actual position of the AR vs. its reference position. In the bottom plot we report a coordinate of the estimated force, due to the contact with the human, along the x-axis of the world frame. Note the change in the position reference in response to the estimated force.

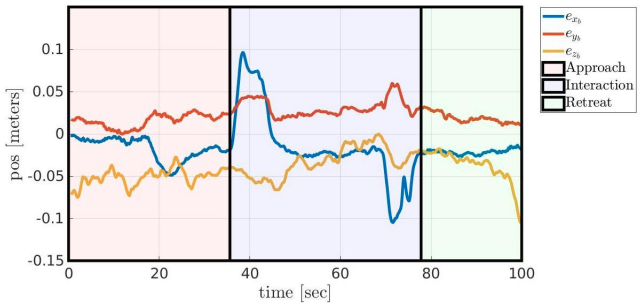

Fig. 6. In this figure, we report the position tracking errors of the aerial robot, throughout the experiment. In general the motion controller displays good tracking performance.

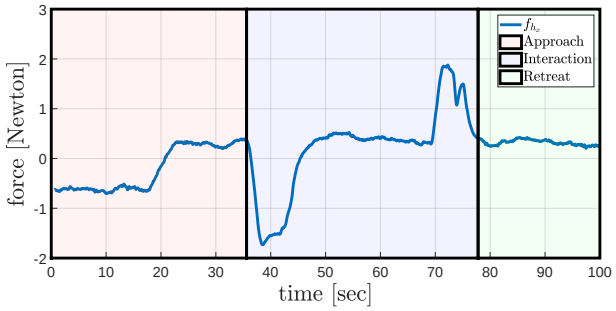

Fig. 7. In this plot, we demonstrate a side effect of using a model-based wrench estimator. Due to model uncertainties, a non-zero force is estimated even when there is no contact. This problem is generally resolved using thresholds, which has consequences on the sensitivity of the robot to the contact forces.

In this application, the robot's desired interaction behavior is to enable the human to manually guide and position the it in space. This is achieved by choosing desired admittance parameters and updating the desired aerial vehicle position within the admittance filter to the current estimated position.

As mentioned in Sec. IV the platform is anchored to the ceiling by means of a cable. Therefore the experimental setup induces an external disturbance on the platform. We evaluated experimentally that the main components of the disturbance affect the robot mainly along the y and z-axis in the world frame, in addition to the rotational degrees of freedom. Therefore in the experiment, the desired admittance behavior is only enabled along the x-axis in the world frame. Otherwise, the robot exhibits a stiff behavior in the remaining DoFs. The x-axis of F_w is aligned with the direction that corresponds to the aerial vehicle moving sideways in-front of the human.

After the approach phase, the human performing the experiment signals the intention to physically interact with the robot. The state machine is changed to the interaction state. This means that the estimated interaction wrench is fed to the admittance filter allowing the aerial robot to implement the desired admittance behavior given by the selected admittance parameters.

The human re-positions the robot in space by manually guiding it to a preferred position. By examining the interaction phase in the top and bottom plots of Fig. 5. We see that from approximately $t = 37s$ to $t = 43s$, the robot implements the desired admittance behavior (see top plot in Fig. 5), in response to the estimated interaction wrench which can be appreciated in the bottom plot of Fig. 5. At this stage, the human proceeds to attach a tool to the end effector of the robot. Since, attaching the payload does not have any effect on the estimated f_{h_x}, the admittance filter does not change the reference set-point along the x-axis. This is followed by another re-positioning of the robot, which is displayed in Fig. 5 approximately from $t = 65s$ to $t = 77s$

Another very important point is that due to model uncertainty and disturbances, the wrench observer can output a non-zero estimate of the external wrench even in the absence of interaction forces. This is a known issue of the external wrench estimation [18], which can be solved by using some thresholds. In Fig. 7, we report the external force estimated without applying a threshold. The signal obtained after applying the threshold is depicted in the bottom plot of Fig. 5 . The consequences of this issue will be discussed in the Sec. VI.

Finally, once the interaction phase is over, the human signals to the supervisor, who initiates the retreat phase, as shown in Fig. 5.

VI. Discussion, Insights & Conclusions

The experiments in Sec. V show that, thanks to the recent progress in field of aerial physical interaction, the control methods and the hardware designs available allow to start considering the problem of pHARI. These experiments, in our opinion, also highlight some of the limitations of the state-of-the-art and shed light on the main new challenges to be addressed in the future. In this section, we discuss the lessons learned from these experiments, with the objective of giving insights into possible future research directions.

A. Challenges for contact wrench estimation in pHARI realistic scenarios

In Sec. V, we highlighted the effects that model uncertainty and external disturbances have on the estimated external wrench. In a realistic scenario involving interacting with a worker at height, the interaction would usually take place in an outdoor environment where the wind action would be non-negligible. Consequently, the disturbances induced by the wind gusts will influence the estimation of the contact wrenches. An initial treatment of this problem has been proposed in [19], the authors provide multiple methodologies to distinguish the contact forces and moments from the wrench applied by the wind on the robot. Their methodologies were mostly tested in simulation and considered a quadrotor platform without a robotic arm. A different approach to the contact wrench estimation would be the use of a force-torque sensor such as in [20], where this kind of sensor is placed at the end effector of an aerial manipulator and is used in physical interaction experiments. However, the experimental campaign is performed in an indoor environment, therefore, the sensor effectiveness outdoor is yet to be tested. Additionally, having a force-torque sensor would limit the identifiable contact wrench to the point where the sensor is mounted, which might consequently limit the flexibility of the interaction.

An equally important open point is how to handle payloads in this control architecture. For the AM to become an aerial co-worker, it must carry tools and help in transporting objects. In our experiments, we relied on the motion controller performance to cancel out the external disturbances due to the extra payload, which weighted approximately $0.2\,\mathrm{kg}$. However, this might prove ineffective with larger payloads.

Therefore, A robust contact wrench estimation approach that can handle disturbances, payloads and wind effects in a versatile manner is needed. Perhaps even combining force-torque sensing capabilities and data-driven techniques.

B. The consequences of a servo-controlled robotic arm, for an aerial interaction task

As mentioned in Sec. II, the robotic arm is controlled using servo motors that can be commanded with a position or velocity commands. This characteristic limits the effectiveness of any interaction control methods which requires force/acceleration commands such as impedance or admittance control. This issue has been tackled in the domain of ground mobile manipulators, where the mobile base is velocity controlled while the robotic arm is torque-controlled [13]. The solution proposed in [13] is to use an admittance interface to the velocity controlled part of the system, the mobile base in this case. However, this method relies on the assumption that we presented in (7).

So far, aerial platform payload restrictions have led to robotic arm designs that require light weight servo motors. However, with aerial physical interaction tackling more challenging problem such as pHARI, there is a need for robotic arms that allow accurate control of generalized forces. one such example can be found in the legged locomotion community [21].

C. On the exploitation of kinematic redundancy in aerial manipulators

The AM platform presented in in Sec. II, has 9 DoFs, which makes the robot redundant w.r.t. to a 6 DoFs EE task. In this work, we did not consider the system redundancy which can prove very interesting or even vital for the interaction with humans. One can consider, for example, using the AM redundancy to maximize the distance between the propellers and the human. However, in the context of operational space control [22] (for example, control of the EE), the exploitation of an AM kinematic redundancy is particularly challenging. One has to devise redundancy resolution methods that do not compromise the stability of the aerial platform. One concrete example, that pertains to the fully-actuated platform used in this work can be seen in [23], in which the projection in the null space approach is used to improve the stability of the platform based on a heuristic. In our opinion, in order to effectively exploit an AM's redundancy, the constraints given by the system dynamics and actuator limits must be taken into account, for example, by using optimization based approaches.

Another interesting and important point in pHARI is the system's tolerance to rotor failure. In the case where an AM is collaborating physically with a human, it will be important that the robot can, at least control its EE position, in the case of rotor failure. Fully actuated aerial platforms have the advantage of being able to statically hover in case of loss of a rotor. However, to maintain EE position in that scenario, kinematic redundancy would be needed. Similar arguments have been made for ground manipulators [24] and it would be interesting to see how such methods can be used for AMs.

D. Conclusions

In summary, we presented the concept of an aerial co-worker for operations at height as a new interesting application in aerial robotics. By using state-of-the-art methods in aerial physical interaction, we performed a first of its kind pHARI experiment with a complex aerial manipulator platform. Our experiments show the viability of the application and explore the effectiveness of adopting state-of-the-art methods. Our results led to a number of insights and new open problems that can direct the future of research to realize aerial robots that can collaborate and coexist with humans.

REFERENCES

[1] M. Tognon, H. A. Tello Chávez, E. Gasparin, Q. Sablé, D. Bicego, A. Mallet, M. Lany, G. Santi, B. Revaz, J. Cortés, and A. Franchi, "A truly redundant aerial manipulator system with application to push-and-slide inspection in industrial plants," *IEEE Robotics and Automation Letters*, vol. 4, no. 2, pp. 1846–1851, 2019.

[2] J. Cacace, S. M. Orozco-Soto, A. Suarez, A. Caballero, M. Orsag, S. Bogdan, G. Vasiljevic, E. Ebeid, J. A. A. Rodriguez, and A. Ollero, "Safe local aerial manipulation for the installation of devices on power lines: Aerial-core first year results and designs," *Applied Sciences*, vol. 11, no. 13, p. 6220, 2021.

[3] T. Bartelds, A. Capra, S. Hamaza, S. Stramigioli, and M. Fumagalli, "Compliant aerial manipulators: Toward a new generation of aerial robotic workers," *IEEE Robotics and Automation Letters*, vol. 1, no. 1, pp. 477–483, 2016.

[4] S. Rajappa, M. Ryll, H. H. Bülthoff, and A. Franchi, "Modeling, control and design optimization for a fully-actuated hexarotor aerial vehicle with tilted propellers," in *2015 IEEE Int. Conf. on Robotics and Automation*, Seattle, WA, May 2015, pp. 4006–4013.

[5] M. Hamandi, F. Usai, Q. Sable, N. Staub, M. Tognon, and A. Franchi, "Design of multirotor aerial vehicles: a taxonomy based on input allocation," *The International Journal of Robotics Research*, vol. 40, no. 8-9, pp. 1015–1044, 2021.

[6] G. Antonelli, E. Cataldi, G. Muscio, M. Trujillo, Y. Rodriguez, F. Pierri, F. Caccavale, A. Viguria, S. Chiaverini, and A. Ollero, "Impedance control of an aerial-manipulator: Preliminary results," in *2016 IEEE/RSJ Int. Conf. on Intelligent Robots and Systems*, Daejeon, South Korea, 2016, pp. 3848–3853.

[7] M. Ryll, G. Muscio, F. Pierri, E. Cataldi, G. Antonelli, F. Caccavale, D. Bicego, and A. Franchi, "6D interaction control with aerial robots: The flying end-effector paradigm," *The International Journal of Robotics Research*, vol. 38, no. 9, pp. 1045–1062, 2019.

[8] L. Peric, M. Brunner, K. Bodie, M. Tognon, and R. Siegwart, "Direct force and pose nmpc with multiple interaction modes for aerial push-and-slide operations," in *2021 IEEE Int. Conf. on Robotics and Automation*. IEEE, 2021, pp. 131–137.

[9] R. Rashad, D. Bicego, J. Zult, S. Sanchez-Escalonilla, R. Jiao, A. Franchi, and S. Stramigioli, "Energy aware impedance control of a flying end-effector in the port-Hamiltonian framework," *IEEE Trans. on Robotics*, 2022.

[10] A. Ollero, M. Tognon, A. Suarez, D. J. Lee, and A. Franchi, "Past, present, and future of aerial robotic manipulators," *IEEE Trans. on Robotics*, vol. 38, no. 1, pp. 626–645, 2021.

[11] F. Augugliaro and R. D'Andrea, "Admittance control for physical human-quadrocopter interaction," in *2013 European Control Conference (ECC)*. IEEE, 2013, pp. 1805–1810.

[12] M. Tognon, R. Alami, and B. Siciliano, "Physical human-robot interaction with a tethered aerial vehicle: Application to a force-based human guiding problem," *IEEE Trans. on Robotics*, vol. 37, no. 3, pp. 723–734, 2021.

[13] A. Dietrich, K. Bussmann, F. Petit, P. Kotyczka, C. Ott, B. Lohmann, and A. Albu-Schäffer, "Whole-body impedance control of wheeled mobile manipulators," *Autonomous Robots*, vol. 40, no. 3, pp. 505–517, 2016.

[14] M. Orsag, C. Korpela, P. Oh, S. Bogdan, and A. Ollero, *Aerial Manipulation*. Springer, 2018.

[15] T. Lee, M. Leoky, and N. H. McClamroch, "Geometric tracking control of a quadrotor UAV on SE(3)," in *49th IEEE Conf. on Decision and Control*, Atlanta, GA, Dec. 2010, pp. 5420–5425.

[16] G. Corsini, M. Jacquet, A. E. Jimenez-Cano, A. Afifi, D. Sidobre, and A. Franchi, "A general control architecture for visual servoing and physical interaction tasks for fully-actuated aerial vehicles," in *1st Work. on Aerial Robotic Systems Physically Interacting with the Environment*, Biograd na Moru, Croatia, Oct. 2021.

[17] T. Tomić, C. Ott, and S. Haddadin, "External Wrench Estimation, Collision Detection, and Reflex Reaction for Flying Robots," *IEEE Trans. on Robotics*, vol. 33, no. 6, pp. 1467–1482, 2017.

[18] S. Haddadin, A. De Luca, and A. Albu-Schäffer, "Robot collisions: A survey on detection, isolation, and identification," *IEEE Transactions on Robotics*, vol. 33, no. 6, pp. 1292–1312, 2017.

[19] T. Tomić, P. Lutz, K. Schmid, A. Mathers, and S. Haddadin, "Simultaneous contact and aerodynamic force estimation (s-CAFE) for aerial robots," *The International Journal of Robotics Research*, vol. 39, no. 6, pp. 688–728, 2020.

[20] G. Nava, Q. Sablé, M. Tognon, D. Pucci, and A. Franchi, "Direct force feedback control and online multi-task optimization for aerial manipulators," *IEEE Robotics and Automation Letters*, vol. 5, no. 2, pp. 331–338, 2020.

[21] F. Grimminger, A. Meduri, M. Khadiv, J. Viereck, M. Wüthrich, M. Naveau, V. Berenz, S. Heim, F. Widmaier, T. Flayols, J. Fiene, A. Badri-Spröwitz, and L. Righetti, "An open torque-controlled modular robot architecture for legged locomotion research," *IEEE Robotics and Automation Letters*, vol. 5, no. 2, pp. 3650–3657, 2020.

[22] O. Khatib, "A unified approach for motion and force control of robot manipulators: The operational space formulation," *IEEE Journal on Robotics and Automation*, vol. 3, no. 1, pp. 43–53, 1987.

[23] A. Afifi, M. van Holland, and A. Franchi, "Toward physical human-robot interaction control with aerial manipulators: Compliance, redundancy resolution, and input limits," in *2022 IEEE Int. Conf. on Robotics and Automation*, Philadelphia, PA, May 2022.

[24] C. L. Lewis and A. A. Maciejewski, "Fault tolerant operation of kinematically redundant manipulators for locked joint failures," *IEEE Transactions on Robotics and Automation*, vol. 13, no. 4, pp. 622–629, 1997.